International Journal of Thermophysics, Vol. 28, No. 1, February 2007 (© 2006)
DOI: 10.1007/s10765-006-0126-2

Numerical Analysis of Piezoelectric Spectra of $Zn_{1-x-y}Be_xMn_ySe$ Mixed Crystals

M. Maliński,[1] J. Zakrzewski,[2,3] and K. Strzałkowski[2]

Received April 25, 2006

This article presents the numerical analysis of the amplitude and phase piezoelectric spectra of a group of mixed crystals of the $Zn_{1-x-y}Be_xMn_ySe$ type. After growth treatment of mixed crystals, such as grinding, polishing, and etching, some surface defects have been created whose energy levels are in the region of the band gap of the material. The lower the concentration of these defects is, the smaller amplitude of the photothermal signal in this energy region is expected and the higher the quality of such a crystal surface is. This article focused on the study of the application of photothermal piezoelectric method for investigation of the surface energy levels and their corresponding absorption bands in the energy-gap region of the material.

KEY WORDS: mixed crystals; piezoelectric detection; semiconductors.

1. INTRODUCTION

Photothermal methods [1] have recently become a very useful tool for measurements of the optical and thermal parameters of semiconductors [2,3,5]. The significance of thermal phenomena becomes more and more important because of the problem of energy dissipation in miniaturized semiconducting devices. One of the thermal methods is the piezoelectric photothermal (PZE) technique which was developed by Jackson and Amer [6] and by Blonskij et al. [7]. This method was successfully used to investigate the properties of A2B6 mixed crystals [8,9]. It was also applied for

[1] Department of Electronics, Technical University of Koszalin, ul. Śniadeckich 2, 75–328 Koszalin, Poland.
[2] Instytut Fizyki, Uniwersytet Mikołaja Kopernika, ul. Grudziądzka 5/7, 87–100 Toruń, Poland.
[3] To whom correspondence should be addressed. E-mail: jzakrzew@phys.uni.torun.pl

measurements of piezoelectric (PZE) spectra of other semiconductors such as CdTe, CdS:Se, GaAs, or Si [10–19]. In general, the piezoelectric method takes advantage of processes that occur in solid-state samples heated by a periodically modulated beam of light. As a result of periodical heating, a spatial and temporal temperature field arises in the sample. This temperature field induces thermal expansion of the sample causing both the so-called piston and drum effects. A piston effect describes a thermal linear expansion of the sample resulting in periodical changes of the thickness of the sample while the drum effect describes the periodical thermoelastic bending of the sample. In piezoelectric experiments the sum or difference of these two effects are observed simultaneously depending on the applied experimental configuration.

Interpretation of the piezoelectric amplitude and phase spectra of semiconductors requires a special numerical approach. The dependence of the amplitude and phase spectra of the piezoelectric signals on the value of the optical absorption coefficient is strongly nonlinear. Additional difficulty arises from the fact that analyzed crystals are often not perfect, which results in the necessity of the development of special numerical models for interpretation of the spectra. Theoretical details concerning some aspects of computations of piezoelectric spectra in the rear and front configurations were presented in previous papers [20–22].

ZnSe-based diluted magnetic semiconductors (DMS) obtained by alloying with Be and Mn chalcogenides are studied intensively because of their high potential application in spintronics. Among them, the $Zn_{1-x-y}Be_xMn_ySe$ quaternary is particularly interesting because a partial substitution of Zn by Be allows for control of the structure (lattice constant) and energy gap of the material.

2. SAMPLE PREPARATION AND MEASURING METHOD

$Zn_{0.75}Be_{0.05}Mn_{0.20}Se$ and $Zn_{0.85}Be_{0.05}Mn_{0.10}Se$ crystals were grown from high-purity powder using the high-pressure Bridgman method. The as-grown crystals were single phase. For the investigated samples no compositional disorders for the compositional parameters x and y were observed in the bulk matrix region. If there was a fluctuation in the x parameter, then these regions could affect the piezoelectric signal more than the grain boundaries do. Such compositional disorders were observed and analyzed in other mixed crystals: $Cd_{1-x}Mn_xTe$ and $Zn_{1-x}Be_xTe$ [23, 24].

The crystal rod was cut into about 1 mm thick samples which were first ground using grinding powder (10μ m diameter), then polished with diamond paste (1μ m), and finally chemically etched. A solution of

H_2SO_4(96%), $K_2Cr_2O_7$, and water was used for etching the samples. After etching, the samples were rinsed in distilled water and then immersed for a few seconds in boiling NaOH. Then the samples were rinsed again in cold water, next in boiling distilled water, and finally in ethyl alcohol.

In the PZE experiment samples were illuminated with the intensity modulated beam of light of a xenon lamp (Cermax 300 W) after passing through the prism monochromator. The piezoelectric signal was detected with a lock-in phase selective amplifier (Stanford SR 510). The piezoelectric characteristics were measured at room temperature in the rear and front experimental configurations [25]. All measurements were computer controlled. A schematic diagram of the piezoelectric cell and applied experimental rear and front configurations is shown in Fig. 1. This construction is advantageous because it gives a PZE signal several times larger than in the case of a ring-shape detector used for the front configuration to date. In the applied configuration, in the region of small optical absorption, the PZE detector is not illuminated with a beam of light. Moreover, one does not have to change a PZE detector or the sample when he/she

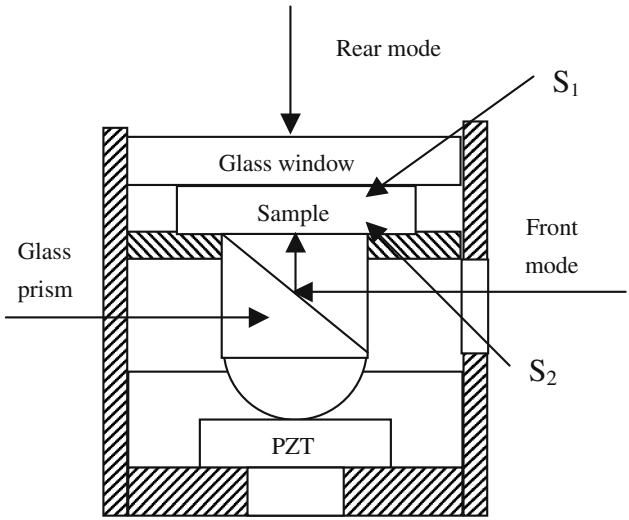

Fig. 1. Schematic diagram of the glass prism PZE cell used in the experiments. It enables both rear and front configuration measurements. PZE means a PZE transducer. Upper surface of the sample, illuminated in the rear configuration, denoted as S_1, corresponds to a value of the spatial coordinate $x = 0$. Bottom side of the sample, denoted as S_2, corresponds to a value of x $= l$, where l is the thickness of a sample.

changes configurations from rear to front. The only necessary change is a change in the direction of the beam of light propagation.

3. THEORETICAL MODEL

The analytical dependence of the piezoelectric signal versus the optical absorption coefficient or the energy of the absorbed photons exhibits a strongly nonlinear character. It is connected, among others, with the complex mechanism of the generation of the piezoelectric signal. The periodical changes of the temperature field in the sample are the result of the absorption of the periodically modulated beam of light. The character of the temperature field depends on the modulation frequency, thermal diffusivity of the material of the sample, optical absorption coefficient spectrum of the material, the thickness of the sample, and the thermal reflection coefficient between the sample and the backing material [20]. For the present case, the value of the thermal diffusivity of the investigated samples was estimated from the fitting of theoretical phase PZE curves to experimental data with $\alpha = 0.03\,\mathrm{cm}^2 \cdot \mathrm{s}^{-1}$.

The temperature field exhibits a thermal wave character and can be computed with a thermal wave interference approach as a result of interference of several thermal wave contributions [26]. The general formula describing the periodical contribution of the temperature field in the sample was derived with the thermal wave interferometry method [20]. This periodical temperature distribution in the sample results in its periodical thermal expansion and thermoelastic bending which are detected by means of a piezoelectric transducer.

For the investigated crystals, the theoretical amplitude and phase piezoelectric spectra were computed with two models assuming that either they are single-layer perfect quality crystals or that they exhibit damaged surfaces resulting in, in fact, three-layer samples. The amplitude and phase piezoelectric spectra presented in this paper were computed for the rear experimental configuration with the expression given by the one-dimensional (1D) formula presented in previous papers [20,21]. It is a modified Jackson and Amer expression [6];

$$S \cong \frac{1}{l} \int_0^l T(x)dx - \frac{6}{l^2} \int_0^l \left(\frac{l}{2} - x \right) T(x)dx \tag{1}$$

where l is the thickness of a sample, $T(x)$ is the instantaneous temperature spatial distribution $T(x) = T(x, \beta(E), l, f, \alpha)$, x is the spatial coordinate, $\beta(E)$ is the optical absorption coefficient spectrum, f is the

frequency of modulation, and α is the thermal diffusivity of the material. This function, used for computations of the PZE spectra in the band-to-band absorption region, was published previously [20, 21]. The difference between this model and Jackson and Amer's model is that the 1D temperature distribution $T(x)$ applied in the present paper is different from the 3D $T(x,y,z)$ distribution in the paper of Jackson and Amer [6]. The comparison of these two models and the validation of the correctness of a 1D approach were published earlier [27]. Additionally in the present paper the temperature distribution $T(x)$ is, for the first time, the sum of both surface and bulk recombination temperature distributions.

The temperature distribution fields in the sample connected with the surface absorption bands located on the illuminated (at $x=0$) and non-illuminated (at $x=l$) surfaces are given by Eqs. (2) and (3), respectively [20];

$$T_1(x,\beta_{s1}) = \frac{I_0\,(1-\exp(-\beta_{s1}d_1))\,(\exp(-\sigma x)+\exp(-2\sigma l+\sigma x))}{\lambda\sigma\,(1-\exp(-2\sigma l))} \tag{2}$$

$$T_2(x,\beta_{s2}) = \frac{I_0\,(1-\exp(-\beta_{s2}d_2))\,(\exp(-\sigma\,(l-x))+\exp(-2\sigma l+\sigma\,(l-x))}{\lambda\sigma\,(1-\exp(-2\sigma l))} \tag{3}$$

where d_1 and d_2 are thicknesses of surface layers, λ is the thermal conductivity of the material, I_0 is the intensity of light, and σ is a function given by the following relation:

$$\sigma = (1+i)\,(\alpha/\pi f)^{1/2} \tag{4}$$

From Eqs. (2) and (3) one can determine numerically only the values of the products $\beta_{S1}d_1$ and $\beta_{S2}d_2$. Thus, it was assumed in the model that $d_1 = d_2 = 10\mu$ m, and under this assumption, values of β_{S1} and β_{S2} were determined. The surface absorption temperature distributions are different from the bulk absorption results as their temperature spatial decays are determined only by the thermal diffusion and do not depend on the value of the optical absorption coefficient β, as in the case of bulk absorption.

The temperature spatial distribution in the sample, for the case of bulk absorption and the rear configuration, is given by the following expression [20]:

$$\begin{aligned} M(x,\beta) &= \frac{\exp(-\sigma x)-\exp(-x\beta)+\exp[-\sigma(2l-x)]-\exp(-\sigma l+\sigma x-l\beta)+\exp(-2\sigma l-x\beta)-\exp(-\sigma l-\sigma x-l\beta)}{\beta-\sigma} \\ N(x,\beta) &= \frac{\exp(-\sigma x)+\exp(-2\sigma l+\sigma x)-\exp(-2\sigma l-x\beta)+\exp(-\beta x)-\exp[(-(\sigma+\beta)l+\sigma x]-\exp(-\sigma x-\sigma l-l\beta)}{\beta+\sigma} \\ T(x,\beta) &= \frac{\beta I[M(x,\beta)+N(x,\beta)]}{2\lambda\sigma(1-\exp(-2\sigma l)} \end{aligned} \tag{5}$$

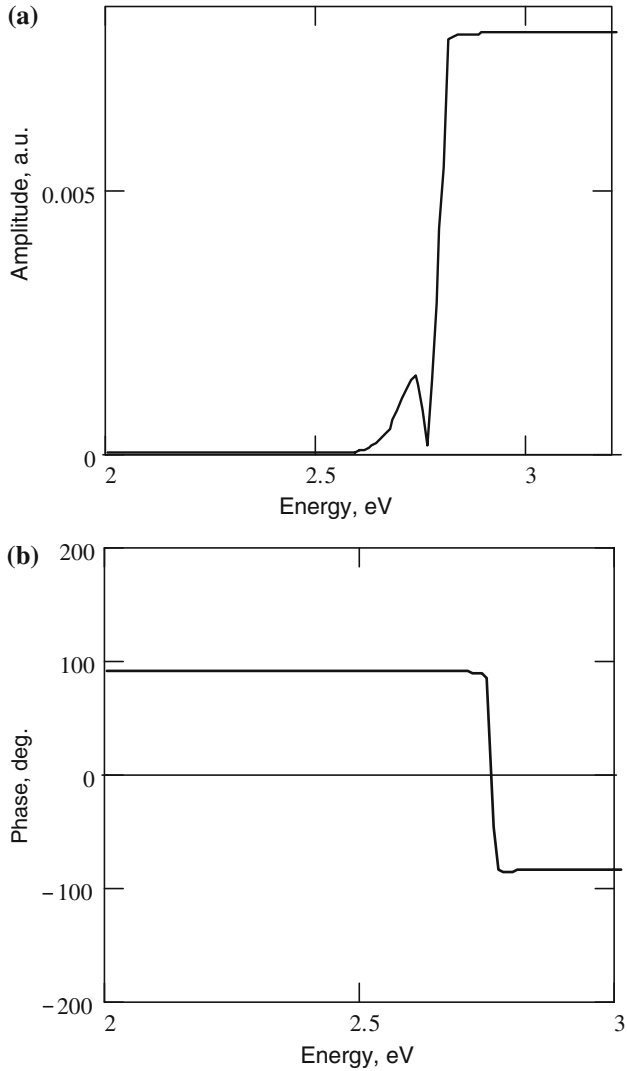

Fig. 2. (a) Amplitude and (b) phase theoretical piezoelectric spectra computed for the rear configuration and a perfect quality crystal, free from surface states, for $f = 76\,\text{Hz}$, $E_g = 2.76\,\text{eV}$, $l = 0.1\,\text{cm}$, and $\alpha = 0.03\,\text{cm}^2 \cdot \text{s}^{-1}$.

The amplitude and phase piezoelectric spectra computed for perfect quality samples in the rear experimental configuration is presented in Figs. 2a and b. The computations were performed with a bulk absorption model where the temperature distribution is described with Eq. (5). The phase in Fig. 2b

remains $+90^\circ$ in the region of low absorption and -90° in the region of high absorption, above the energy gap, 2.76 eV, of a semiconductor, according to the theory of the PZE effect [28]. The small amplitude peak at about 2.65 eV in Fig. 2a is artificial, and it is connected with the rear experimental configuration. In this configuration the PZE signal is the difference of the piston and drum contributions. At 2.65 eV this difference reaches a maximum, and at about 2.75 eV, these two contributions cross and the difference reaches a minimum. Real crystals can exhibit, however, surface levels responsible for corresponding surface absorption bands located in the energy gap of a semiconductor on one or both surfaces. Let us consider the surface absorption band located on the S_1 side of the sample with the energy maximum E_1 and the sample measured in the rear experimental configuration. A schematic diagram of such a sample is presented in Fig. 3.

The optical absorption coefficient spectrum for the energy region below the energy gap was modeled with the Gaussian type function, according to Eq. (6) with the maximum $A_0 = 100\,\mathrm{cm}^{-1}$ at $E_1 = 2.2\,\mathrm{eV}$ and $E_{01} = 0.1\,\mathrm{eV}$ presented in Fig. 4a. The corresponding piezoelectric amplitude and phase spectra are presented in Fig. 4b and c.

It is worth noting here that the PZE phase value for $E = 2.2\,\mathrm{eV}$ and for $E > 2.76\,\mathrm{eV}$ are the same although the corresponding optical absorption coefficients are considerably different, 100 and $10000\,\mathrm{cm}^{-1}$, respectively. It is the so-called phase saturation effect. The phase, in the rear configuration,

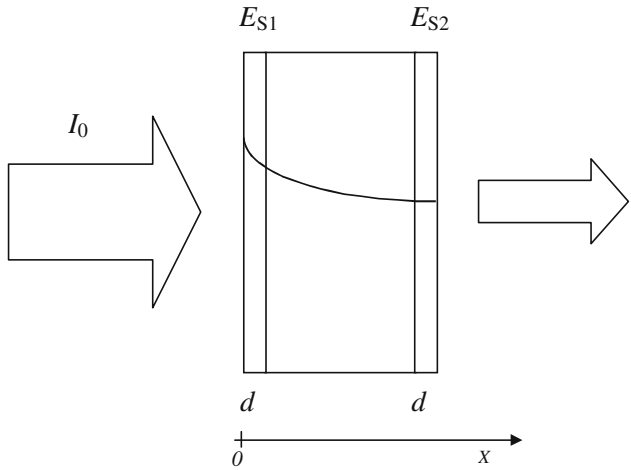

Fig. 3. Schematic diagram of the sample exhibiting surface levels of energy E_{s1} and E_{s2} for rear experimental configuration with the PZE detector located at the non illuminated side of the sample.

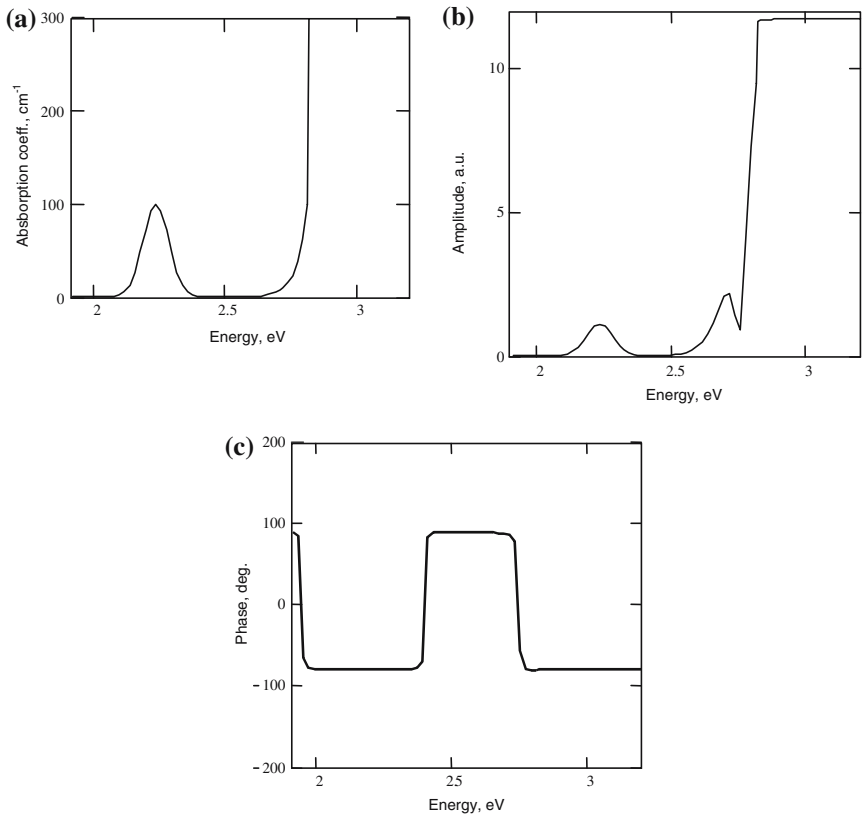

Fig. 4. (a) Optical absorption coefficient spectrum of the sample with the surface absorption band on the S_1 side and (b) its theoretical amplitude and (c) phase PZE spectra computed for the rear configuration and $l = 0.1$ cm, $\alpha = 0.03$ cm$^2 \cdot$ s^{-1}, and $f = 76$ Hz.

can take two levels, $+90^\circ$ and the other in the range from +90 to -90° depending on, among others, the thermal diffusivity of the sample. Practically, there are no intermediate phase levels in PZE phase spectra.

Let the surface absorption band on the S_2 side of the sample (see Fig. 1) exhibit the same energy maximum E_1 and the PZE spectra be computed for the front experimental configuration. Then, in Fig. 5a, b is-presented piezoelectric spectra corresponding to the same optical absorption spectrum as shown in Fig. 4a. Changes of the phase in the front configuration are much smaller. In the high absorption region, above 2.76 eV, the phase tends to $+120^\circ$. For small absorption it changes only to $+90^\circ$. Due to the saturation phase effect, it goes up to $+120^\circ$ again at 2.2 eV as a

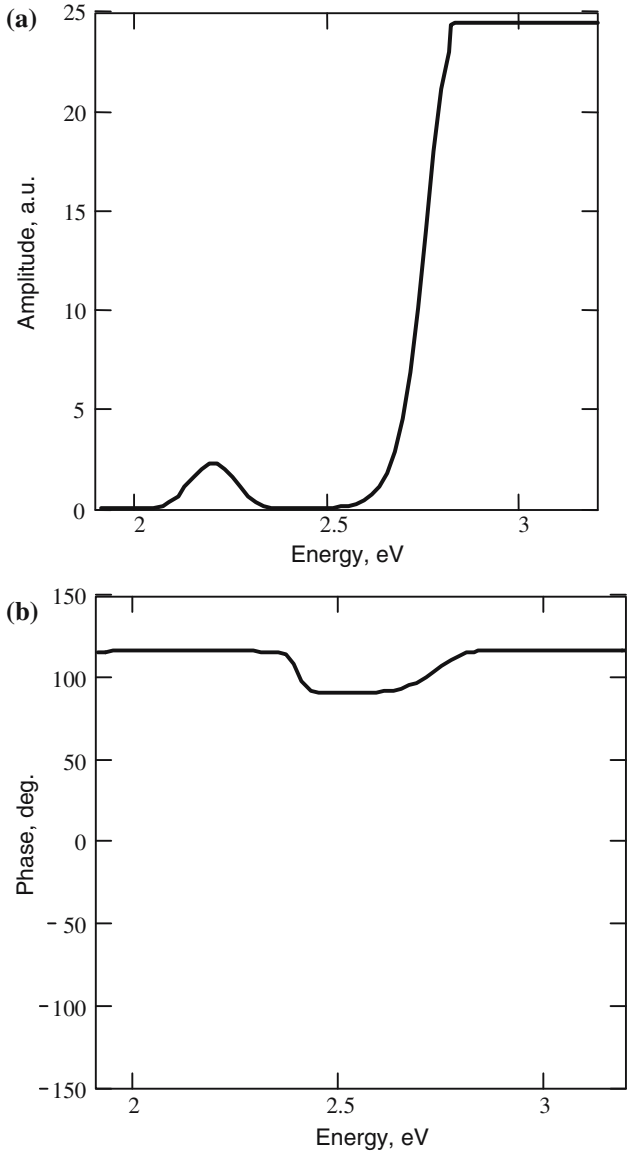

Fig. 5. (a) Theoretical amplitude and (b) phase PZE spectra computed for the front configuration of the sample with the surface absorption band located on the S_2 side of the sample and $l = 0.1$ cm, $\alpha = 0.03$ cm$^2 \cdot$s^{-1}, and $f = 76$ Hz.

result of surface absorption. For small energies of photons, below 1.9 eV, it goes down to $+90^{\circ}$.

In general, the phase shift in PZE spectra can be connected with the change of the nature of the heat sources producing the photothermal signal, and not with the value of the absorption coefficient. An additional heat source associated with the presence of the surface defects influences the temperature distribution and changes the phase of the signal. In the observed spectra (Fig. 4), two-phase shifts can be observed at the boundaries (2 and 2.4 eV) of the Gaussian shape maximum (2.2 eV).

Comparison of the theoretical PZE spectra presented in Figs. 4 and 5 leads to the following conclusions: amplitude spectra computed for the rear and front configurations are very similar and exhibit the maximum 2.2 eV but they do not provide information concerning the spatial location of the defects, whose energy levels are responsible for the absorption bands. The information on energy levels related to the surface states is hidden in the PZE phase spectra. The PZE phase spectrum of the energy level located on the S_1 surface of the sample computed for the rear configuration, presented in Fig. 4c, shows clearly both the absorption band at 2.2 eV and the energy gap at 2.76 eV. When the phase spectrum is computed for the front configuration and the energy level located on the S_2 side of the sample, then neither the energy gap nor the 2.2 eV surface absorption band are clearly visible.

Computations of the piezoelectric spectra for photon energies in the range of the main absorption band were performed for optical absorption coefficient spectra, for the energies below and above the energy gap of the crystal, described with Eqs. (6) and (7) respectively;

$$\beta(E) = \beta_{02} \exp\left(\frac{(E - E_g)\,\gamma}{0.025}\right) \quad \text{for } E < E_g \tag{6}$$

$$\beta(E) = A_2 \left(E - E_g\right)^{1/2} \quad \text{for } E > E_g \tag{7}$$

Equation (6) describes Urbach tail thermal broadening of the absorption band observed for all direct electron-type transition semiconductors. Equation (7) describes the absorption band connected with the direct, band-to-band, electron transitions in semiconductors. The computations were performed for the following set of parameters:

$$\beta_{02} = 100\,\text{cm}^{-1} \quad \gamma = 0.5 \quad E_g = 2.76\ \text{eV} \quad A_2 = 10000\,\text{cm}^{-1}$$

It was assumed that the two optical absorption bands, of the Gaussian type, observed experimentally and connected with the appropriate deep

surface defects, for the energy of photons below the energy gap can be modeled with the following expressions:

$$\beta_{s1}(E) = A_0 \exp\left(-\left(\frac{E - E_1}{E_{01}}\right)^2\right) \tag{8}$$

$$\beta_{s2}(E) = A_1 \exp\left(-\left(\frac{E - E_2}{E_{02}}\right)^2\right) \tag{9}$$

4. EXPERIMENTAL RESULTS

The computations and fits of theoretical characteristics to experimental amplitude and phase PZE spectra for $Zn_{0.75}Be_{0.05}Mn_{0.20}Se$ samples were performed for the following set of parameters of the surface absorption bands:

$$A_0 = 100\,\mathrm{cm}^{-1}, \quad A_1 = 150\,\mathrm{cm}^{-1}, \quad E_1 = 2.20\ \mathrm{eV},$$
$$E_2 = 2.50\ \mathrm{eV}, \quad E_{01} = E_{02} = 0.10\ \mathrm{eV}$$

The average optical absorption coefficient spectrum obtained from the fitting procedures for $Zn_{0.75}Be_{0.05}Mn_{0.20}Se$ samples is presented in Fig. 6.

The piezoelectric, theoretical and experimental, amplitude and phase spectra of $Zn_{0.75}Be_{0.05}Mn_{0.20}Se$ samples measured and computed in the rear configuration are presented in Fig. 7a, b, under the assumption that the energy levels responsible for the 2.2 and 2.5 eV absorption bands are located on different S_1 and S_2 surfaces of the sample, respectively (see Fig. 1). The theoretical and experimental PZE phase spectrum presented in Fig. 7c shows the fit obtained under the assumption that both levels are on the same left side of the sample. This assumption leads to the conclusion that this is not the observed experimental case. The thickness of the sample was $l = 0.1$ cm and the thermal diffusivity $\alpha = 0.03\,\mathrm{cm}^2 \cdot \mathrm{s}^{-1}$. The frequency of modulation was $f = 76$ Hz.

The similar piezoelectric amplitude and phase spectra of the $Zn_{0.75}Be_{0.05}Mn_{0.20}Se$ sample, but measured at $f = 6$ Hz in the rear configuration, and theoretical curves are presented in Fig. 8a and b, respectively.

The PZE spectra of the same sample but measured in the front configuration at $f = 6$ Hz are presented in Fig. 9a, b.

PZE amplitude spectra in both configurations exhibited the following bands: the first band with the maximum at $E_1 = 2.20$ eV and the second one at $E_2 = 2.50$ eV. Numerical simulations indicated also that these

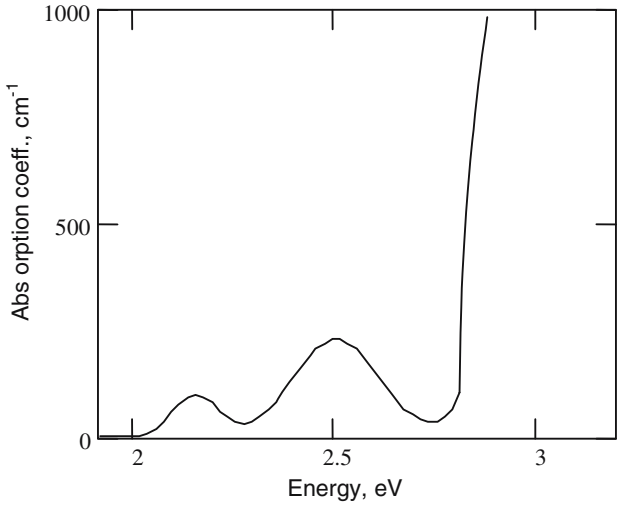

Fig. 6. Average optical absorption coefficient spectrum of the $Zn_{0.75}Be_{0.05}Mn_{0.20}Se$ samples computed from the PZE spectra measured at different frequencies of modulation and configurations.

bands are located on surfaces of the samples and not inside the crystals. From an analysis of the PZE phase spectra, it was also possible to establish that the corresponding levels were localized on different surfaces of the samples not on the same surface. The energy levels at $E_1 = 2.2\,\text{eV}$ were located on the illuminated S_1 surface of the sample while the energy levels at $E_2 = 2.5\,\text{eV}$ were located on the S_2 surface of the sample. Moreover, the analysis of the spectra indicated that only the band with the maximum at 2.2 eV, located on the S_1 side of the sample, can be detected with the PZE phase spectra independently of the experimental configuration. On the contrary, the band with the maximum at 2.5 eV located on the S_2 side of the sample, exhibits an almost constant phase of about $+90^\circ$ and cannot or hardly be visible in the phase spectra, independent of the experimental configuration. It was also possible to estimate roughly the values of the optical absorption coefficient involved with these absorption bands to be about 100 and $150\,\text{cm}^{-1}$, respectively.

The piezoelectric amplitude and phase, theoretical and experimental, spectra of the $Zn_{0.85}Be_{0.05}Mn_{0.10}Se$ crystal sample are presented in Fig. 10a, b. They were measured in the rear configuration. These amplitude spectra exhibit two different absorption bands below the energy gap of the crystal located at $E_1 = 2.35\,\text{eV}$ and $E_2 = 2.60\,\text{eV}$. The phase spectra

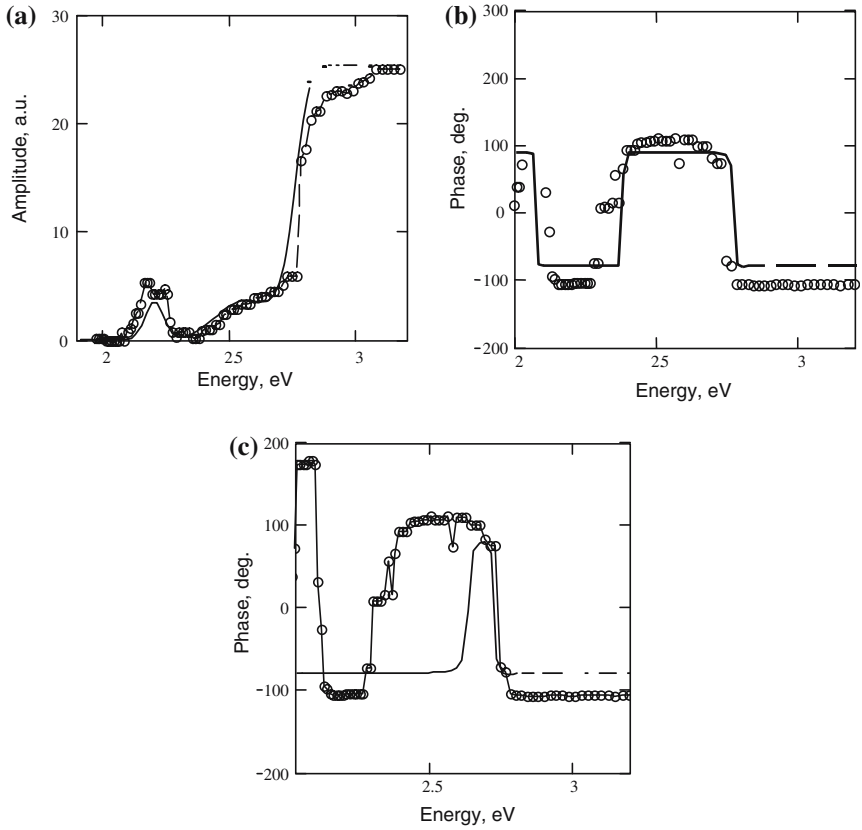

Fig. 7. Experimental and theoretical PZE (a) amplitude and (b) phase spectra of a $Zn_{0.75}Be_{0.05}Mn_{0.20}Se$ sample for $f = 76$ Hz in the rear configuration when the 2.2 eV absorption band is on the S_1 surface and the 2.5 eV absorption band is on the S_2 surface of the sample (see Fig. 1). (c) Theoretical PZE phase spectrum computed for the rear configuration under the assumption that 2.2 and 2.5 eV absorption bands are on the same S_1 surface. Circles show experimental results, and solid lines represent theoretical curves.

revealed that both absorption bands were located this time on the same side of the sample and their corresponding absorption band spectrum determined from the fitting procedure is presented in Fig. 10c. These surface absorption bands can be described by the set of parameters:

$$A_0 = 350\,\mathrm{cm}^{-1}, \quad A_1 = 260\ \mathrm{cm}^{-1}, E_1 = 2.35\ \mathrm{eV}, \quad E_2 = 2.60\ \mathrm{eV}, E_{01} = E_{02} = 0.15\ \mathrm{eV}$$

The physical nature of these surface absorption bands is not known at present and is the subject of current investigations.

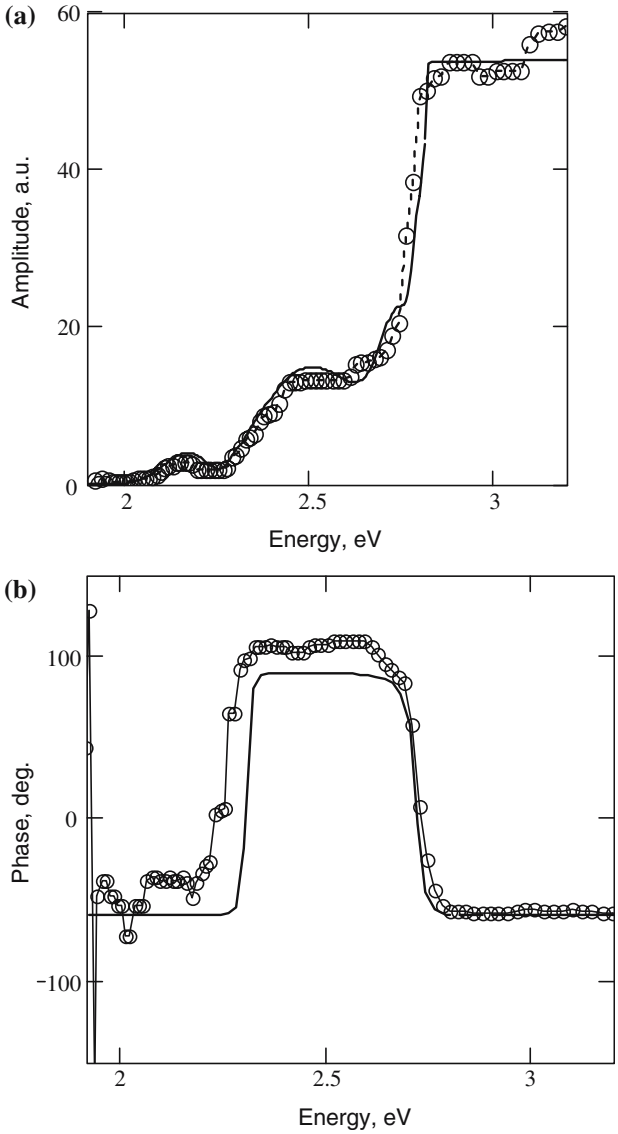

Fig. 8. (a)**A**mplitude and (b) phase experimental and theoretical piezoelectric spectra of a $Zn_{0.75}Be_{0.05}Mn_{0.20}Se$ sample for f = 6 Hz, in the rear configuration. Circles show experimental results, and solid lines represent theoretical curves. 2.2 and 2.5 eV absorption bands are on S_1 and S_2 surfaces, respectively (see Fig. 1).

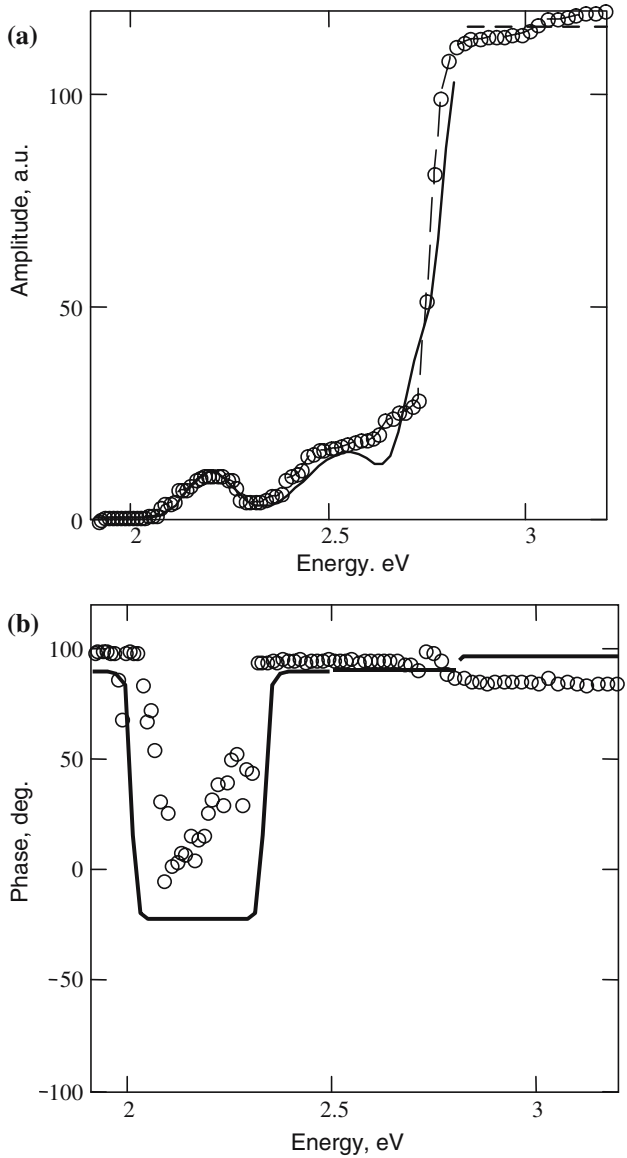

Fig. 9. (a) Amplitude and (b) phase experimental and theoretical piezoelectric spectra of a $Zn_{0.75}Be_{0.05}Mn_{0.20}Se$ sample in the front configuration for $f = 6$ Hz. Surface 2.2 and 2.5 eV absorption bands are located on S_1 and S_2 surfaces, respectively (see Fig. 1). Circles show experimental results, and solid lines represent theoretical curves.

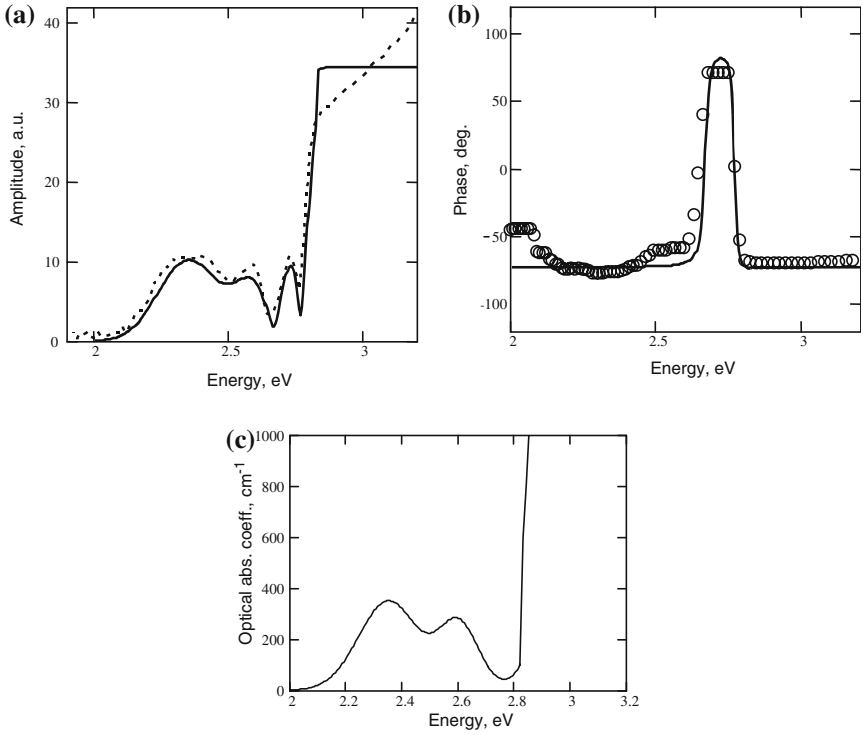

Fig. 10. (a) Amplitude and (b) phase experimental and theoretical piezoelectric spectra of a $Zn_{0.85}Be_{0.05}Mn_{0.10}Se$ sample in the rear configuration for $f = 76\,\text{Hz}$. Surface absorption bands at 2.36 and 2.60 eV are located on the same S_1 surface (see Fig. 1). Circles show experimental results, and solid lines represent theoretical curves. (c) Optical absorption coefficient spectrum of the sample determined from the amplitude PZE spectrum.

5. CONCLUSIONS

Piezoelectric (PZE) spectra of semiconductor samples were measured, computed and analyzed in detail, and the experimental spectra with theoretical fittings are presented in the paper. The results of computations, performed in a developed one dimensional Jackson and Amer model [6], shown in this article, demonstrate that the piezoelectric method is also useful for the analysis of low optical absorption coefficient spectra in the energy regions below the energy gap of semiconductors. It is essential from the point of view of estimation of the quality of mixed crystals or the quality of the state of their surfaces. Due to the enhancement effect of the PZE detection for the low optical absorption values and the saturation effect for the high absorption values, this method is

advantageous for measurements of low absorption bands. Applying this method for investigations of $Zn_{0.75}Be_{0.05}Mn_{0.20}Se$ and $Zn_{0.85}Be_{0.05}Mn_{0.10}Se$ crystals, it was possible to detect absorption bands located below the energy gap of the material. It also results from the present studies that the PZE phase spectra turned out to be a source of information about the spatial location of defects responsible for observed absorption bands. Analysis of the phase spectra allows determination of which side of the sample they are located even if the amplitude PZE spectra are very similar. For the purpose of confirmation of the conclusions drawn from the analysis of the PZE spectra, surfaces of the samples were treated mechanically: roughened, polished, and finally etched. After each process, the PZE spectra were recorded. These experiments confirmed that the 2.2, 2.36, 2.5, and 2.60 eV absorption bands are connected with the quality of the surface. Due to the short lifetime of excess carriers in A2B6 semiconductors, about 10^{-9} s, and low frequencies of modulation used in the presented experiments the plasma effect could be neglected. The plasma wave effect must be considered when PZE experiments are performed at frequencies above 10 kHz, but not at low frequencies and thick samples. This problem has already been analyzed for A2B6 semiconductors and described in several papers, among others [29, 30].

The results of this research lead to the conclusion that the piezoelectric method can be applied successfully for the testing procedure in examination of the quality of surfaces of semiconductor samples after surface treatment procedures. This approach will be applied in the future for the purpose of examination and comparison of the quality of surfaces of mixed crystals after different etching procedures.

ACKNOWLEDGMENTS

This work was supported in part by the Committee for Scientific Research (Poland) under the grant No: 1 P03B 092 27 (2004–2007) and in part by Uniwersytet Mikolaja Kopernika w Toruniu under grant No: 384-F.

REFERENCES

1. A. Rosencwaig and A. Gersho, *J. Appl. Phys*. **47:**64 (1976).
2. A. Mandelis, J. Batista, and D. Shaughnessy, *Phys. Rev. B* **67:**205208–1 (2003).
3. A. Memon, A. Fukuyama, S. Sato, and T. Ikari, *Rev. Sci. Instrum*. **74:**592 (2003).
4. D. Dietzel, S. Chotikaprakhan, B. K. Bein, and J. Pelzl, *J. Phys. IV France* **125:**87 (2005).
5. D. M. Todorovic, *Rev. Sci. Instrum.* **74:**582 (2003).
6. W. Jackson and N. M. Amer, *J. Appl. Phys*. **51:**3343 (1980).

7. J. V.Blonskij, V. A. Tkhoryk, and M. L. Shendeleva, *J. Appl. Phys.* **79:**3512 (1996).
8. M. Maliński and J. Zakrzewski, *Rev. Sci. Instrum.* **74:**598 (2003).
9. J. Zakrzewski, M. Pawlak, F. Firszt, S. Łêgowski, A. Marasek, H. Mêczyńska, and M. Maliński, *Int. J. Thermophys.* **26:**285 (2005).
10. T. Hata, Y. Sato, and M. Kurebayashi, *Jpn. J. Appl. Phys*. **22:**205 (1983).
11. T. Hata, Y. Sato, Y. Nagai, and T. Hada, *Jpn. J. Appl. Phys*. **23:**75 (1984).
12. O. Goede, W. Heimbrodt, and Th. Kopp, *Phys. Status Solidi A* **108:**443 (1988).
13. O. Goede, W. Heimbrodt, and F. Sittel, *Phys. Status Solidi A* **93:**277 (1986).
14. T. Ikari, K. Miyazaki, A. Fukuyama, H. Yokoyama, K. Maeda, and K. Tutugami *J. Appl. Phys.* **71:**2408 (1992).
15. A. Fukuyama and Y. Akushi, *Phys. Rev. B* **58:**12868 (1998).
16. K.Wasa, K.Tsubouchi, and N. Mikoshiba, *Jpn. J. Appl. Phys*. **19:**L475 (1980).
17. T. Ikari, A. Fukuyama, K. Maeda, and K. Futagami, *Phys. Rev. B* **46:**10173 (1992).
18. T. Ikari, H. Yokoyama, S. Shigetomi, and K. Futagami, *Jpn. J. Appl. Phys.* **29:**887 (1990).
19. M. Maliński and T. Ikari *Microelectronics J*. **34**:1119 (2003).
20. M. Maliński, *Archives of Acoustics* **27:**217 (2002).
21. M. Maliński, *Archives of Acoustics* **28**:43 (2003).
22. M. Maliński, *J. de Phys. IV* **109:**43 (2003).
23. M. Maliński, J. Zakrzewski, S. Łêgowski, and H. Mêczyńska *Int. J. Thermophys.* **26:**255 (2005).
24. M. Malinski and J. Zakrzewski, *Int. J. Thermophys.* **26:**269 (2005).
25. L. Bychto, M. Maliński, J. Zakrzewski, S. Łêgowski, and H. Mêczyńska, *J. de Phys. IV* **117:**25 (2004).
26. C. A. Benett and R. R. Patty, *Appl. Optics* **21:**49 (1982)
27. L. Bychto and M. Maliński, *J. de Phys. IV* **117:**17 (2004).
28. M. Maliński, *Phys. Stat. Sol. (a)* **198:**169 (2002).
29. M. Maliński and L. Bychto, *J. de Phys. IV* **129:**237 (2005).
30. L. Bychto and M. Maliński, *J. de Phys. IV* **129:**213 (2005).